Estimating permeability of sandstone samples by nuclear magnetic resonance and spectral-induced polarization

Andreas Weller[1], Sven Nordsiek[2], and Wolfgang Debschütz[1]

ABSTRACT

Two techniques to estimate permeability are compared in this paper: nuclear magnetic resonance (NMR) and spectral-induced polarization (SIP). Both methods are based on relaxation processes. NMR records the relaxation of hydrogen nuclei after excitation in an external magnetic field. The phenomenon of induced polarization can be characterized by a relaxation of ions after excitation by an electric field. Hydrogen nuclei are concentrated in the pore water, the current flow is restricted to the pore space for most reservoir rocks, and permeability is related to the pore space geometry. Based on the similarity between fluid movement and current flow in the pore space, different relations have been published linking parameters derived from NMR and SIP data to predict permeability.

NMR, SIP and permeability data have been acquired on 53 sandstone samples of the cretaceous Bahariya Formation (Western Desert, Egypt) including 27 samples showing a lamination that causes anisotropy. We compare the applicability of known and generalized relations for permeability prediction including isotropic and anisotropic samples. Because NMR relaxation ignores directionality of pore space geometry, the known relations provide only a weak accuracy in permeability estimation. The integrating parameters derived from a Debye decomposition of SIP data are partly sensitive to anisotropy. A generalized power-law relation using resistivity, chargeability, and mean relaxation time provide a reliable permeability prediction for isotropic and anisotropic samples.

INTRODUCTION

Estimating permeability or hydraulic conductivity using relations that are based on easily measurable parameters is one of the most challenging problems facing petrophysical research. A reliable prediction is of interest for purposes such as formation evaluation of oil and gas reservoirs and the modeling of groundwater flow. For nuclear magnetic resonance (NMR), a correlation between mean relaxation time and permeability is widely applied. Coates et al. (1993) published a study of the relationship between the longitudinal relaxation time T_1 and permeability. Straley et al. (1997) presented a similar equation for the transversal relaxation time T_2.

Laboratory investigations with spectral-induced polarization (SIP) on shaley sands, silt, and clay samples performed by Börner et al. (1996) yield conductivity spectra with a constant phase angle (CPA) behavior in the frequency range between 1 mHz and 1 kHz. Assuming a CPA model, an algorithm for the estimation of hydraulic

conductivity from complex electrical conductivity measured at a single frequency has been developed and successfully tested on borehole and field data (Weller and Börner, 1996). Slater and Glaser (2003) observed that the predictive capability of the so-called Börner model for permeability estimation is restricted to the narrow lithologic range of sandy material. Hördt et al. (2009) summarized the results of several case histories to assess the predictive capability of induced polarization (IP) data to estimate permeability. A reliable determination of small phase shifts for coarse-grained material and uncertainties arising from inversion ambiguity are identified as major problems at the field scale. Because a field survey is restricted to a narrow frequency range, the validity of the CPA model cannot be checked properly. Laboratory investigations cover a wider frequency range providing more information on the spectral behavior of conductivity amplitude and phase shift. Binley et al. (2005) fit Cole-Cole models to IP spectra of saturated and unsaturated sandstones. They emphasize the significance of the time constant determined by

Cole-Cole model fitting for permeability prediction of their samples. Anisotropy of the investigated material only rarely has been considered in permeability prediction. Zisser and Nover (2009) report directional measurements of complex electrical resistivity and permeability for low-permeability sandstone samples. Both time constant and resistivity derived from a Cole-Cole model fitting depend on the considered direction. But an overall relationship between these quantities and permeability could not be observed for absolute values or for their anisotropy.

A data set of 53 sandstone samples of the cretaceous Bahariya formation (Western Desert, Egypt) that has been described in detail by Halisch et al. (2009) was used in our study. Core samples were collected from a drilling site in the Badr El Din concession area in the northwest part of the Abu Gharadig basin. Sampling depths range from 3512 m to 3547 m.

At each depth, a pair of cylindrical samples with a diameter of about 2.5 cm and an average length of 4 cm was extracted from the original drill core. So-called horizontal or H samples have been taken parallel, and so-called vertical or V samples perpendicular to the layering. As shown in Figure 1, the sample set can be subdivided into two major types. Twenty-seven samples belong to the first type that is characterized by visual indications of flaser bedding or lamination structures. Independent of the intensity of flaser bedding structures, all samples of this type are regarded as laminated samples (+L samples). Another 26 samples belong to the second type, that shows no obvious flaser bedding or lamination structures. According to a visual inspection, they can be regarded as pure sandstone samples. This type is referred to as samples without lamination (−L samples).

The depositional environment of the examined samples can be described as an overall transgression with coastal back stepping comprising several coarsening-upward cyclothems. The environment can be characterized as shallow marine with a tidal flat to marine shelf setting. The fine sandy layers of all samples are mainly composed of quartz (70% to 80%), and glauconite (5% to 15%). Cementation minerals are kaolinite and subordinate calcite as well as quartz overgrowths. The brownish flaser bedding is composed of clayey-silty, partly carbonaceous layers that contain many small pyrite framboids and minor rutile. As a result of oxidation, the layers contain minor limonite or other iron minerals, causing a higher volumetric magnetic susceptibility for the +L samples with all values larger than $75 \cdot 10^{-6}$ SI and an average of $148 \cdot 10^{-6}$ SI. The −L samples reach only an average of $60 \cdot 10^{-6}$ SI (Halisch et al., 2009). The conspicuous flaser bedding implicates a distinct anisotropy effect on directional parameters like permeability and electrical resistivity. In general, the +L samples show an anisotropic behavior whereas the −L samples might be regarded as more or less isotropic.

This study investigates the applicability of known and generalized relations using NMR and SIP data for permeability estimation. A novel approach integrates directional and scalar physical parameters determined from IP spectra in relations for permeability prediction. The presented relations aim at an improved permeability prediction for isotropic and anisotropic sandstone samples.

METHODS AND RESULTING PETROPHYSICAL PARAMETERS

Gas permeability and porosity

The permeability of the Bahariya sandstone samples was determined by a gas permeameter using nitrogen as the flowing fluid. Klinkenberg correction has been applied (Scheidegger, 1957). The minima, maxima, average values and standard deviations of the petrophysical parameters, which are relevant for this study, are compiled in Table 1. The resulting permeability values cover four decades in logarithmic scale with a range from 0.007 mD to 56 mD. Lower values were observed for the +L samples with a geometric mean value of 0.126 mD in comparison with a value of 8.02 mD determined for the −L samples.

Permeability is a directional parameter. The permeability K_H measured for a cylindrical H sample in axial direction is equivalent to the longitudinal permeability. V samples provide the transverse permeability K_V. The ratios of the parameters between the horizontal and vertical samples are compiled in Table 2. A strong ratio K_H/K_V, which reflects the degree of anisotropy, is observed for the +L samples with a maximum value of 15.2 and a mean value of 4.53.

Porosity of all samples was determined by triple weighting: in dry state, in fully saturated state, and Archimedes' weighing in a water basin. The porosity varies between 4.9% and 17%, with the lower porosity generally determined for +L samples (see Table 1). Porosity belongs to the scalar parameters that do not depend on the orientation of the sample. Because H and V samples of each pair cannot be regarded as identical twin samples, slight differences in porosity are determined. The ratio Φ_V/Φ_H presented in Table 2 shows values close to 1.0 for the −L samples and a larger variation for the +L samples.

Nuclear magnetic resonance

Because the textbook of Coates et al. (1999) presents an excellent overview on the NMR logging principles, we provide only a short summary of the fundamentals. The nuclear magnetic relaxation of hydrogen in a wetting pore fluid of rocks is controlled by slow relaxation in the free pore fluid and fast relaxation in the direct vicinity of the pore surface. In case of fast diffusion exchange between free pore fluid and the fluid at the pore surface, the magnetization in the pores remains uniform. The relaxation time becomes proportional to the volume-to-surface ratio of the pores or proportional to the radius of pores if a suitable pore model is considered. In rocks with a distribution of pores of varying size, a spectrum of different relaxation times is determined. It can be distinguished between two different types of relaxation times. The longitudinal relaxation time T_1 characterizes the increase of magnetization parallel to the static magnetic field, and the transversal relaxation time T_2 the decrease of magnetization

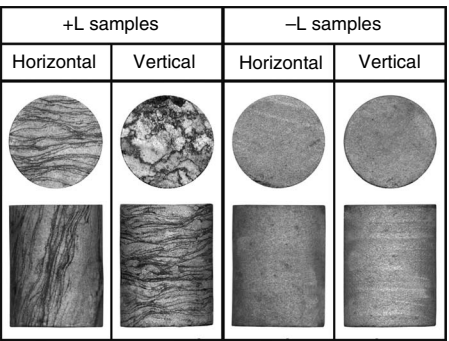| +L samples		−L samples	
Horizontal	Vertical	Horizontal	Vertical

Figure 1. Classification of the cylindrical sandstone samples of Bahariya Formation into horizontal (H) and vertical (V) samples and into laminated (+L) and nonlaminated (−L) samples according to Halisch et al. (2009).

perpendicular to the static magnetic field. Both relaxation times are related to the surface-to-volume ratio S/V by the formula

$$\frac{1}{T_{1,2}} = \beta_{1,2} \times \frac{S}{V} \qquad (1)$$

with β being the surface relaxivity which can be different for T_1 or T_2. No large difference between T_1 and T_2 is observed in free fluids where the relaxation time depends mainly on fluid viscosity. In natural rocks, T_2 is shortened by dephasing effects that are generated by the diffusion of the hydrogen in an inhomogeneous magnetic field as a result of the susceptibility distribution in a microscopically inhomogeneous rock.

The measurement of the NMR relaxation for the two components is different. The longitudinal relaxation time T_1 is measured by the inversion recovery method. T_2 is measured by pulse echo method which is widely known as CPMG pulse sequence (Carr and Purcell, 1954; Meiboom and Gill, 1958). In the case of longitudinal relaxation, the temporal behavior of the amplitude A of the decaying sig-

nal can be presented as an overlay of relaxation processes with different relaxation times T_{1j}

$$A(t) = A_0 \times \sum_{j=1}^{n} a_j \times \left(1 - 2 \times \exp\left(\frac{-t}{T_{1j}}\right)\right). \qquad (2)$$

A similar equation results for the transversal relaxation:

$$A(t) = A_0 \times \sum_{j=1}^{n} a_j \times \exp\left(\frac{-t}{T_{2j}}\right). \qquad (3)$$

The measurement of the inversion recovery is much more time consuming and therefore not applicable in well logging. This is the main reason for the use of T_2 for rock-characterizing relations. To keep the diffusion effect low, a short and constant echo spacing for all regarded samples is necessary. The echo spacing in our investigations was fixed at 600 μs.

In the case of a spectrum of relaxation times, a mean relaxation time

Table 1. Compilation of minimum, maximum, average value, and standard deviation (SD) of petrophysical parameters of all samples, +L, and −L samples (Φ = porosity, K = permeability, $\bar{T}_1$ = mean longitudinal relaxation time, $\bar{T}_2$ = mean transversal relaxation time, ρ_0 = DC resistivity, m_t = total chargeability, $\bar{\tau}$ = mean relaxation time, U_τ = nonuniformity parameter).

Parameter	All samples				+L samples				−L samples			
	min	max	mean	SD	min	max	mean	SD	min	max	mean	SD
Φ	0.049	0.170	0.115	0.033	0.049	0.153	0.095	0.031	0.090	0.170	0.134	0.022
K [mD]	0.007	55.9	0.966	—	0.007	5.58	0.126	—	0.183	55.9	8.02	—
$\bar{T}_1$ [ms]	14.9	209	88.8	61.2	14.9	124	43.3	39.9	47.2	209	133	52.0
$\bar{T}_2$ [ms]	1.21	33.0	9.10	7.58	1.21	13.6	4.36	2.89	4.11	33.0	14.0	7.83
ρ_0 [Ωm]	204	992	473	213	266	992	575	213	204	857	367	156
m_t	0.047	0.269	0.127	0.056	0.109	0.269	0.176	0.031	0.047	0.118	0.078	0.018
$\bar{\tau}$ [ms]	19.0	331	74.5	66.3	24.6	331	105	81.5	19.0	81.3	43.2	15.9
U_τ	1.92	4.23	3.04	0.48	1.92	4.23	3.24	0.53	1.96	3.33	2.83	0.31

Table 2. Compilation of minimum, maximum, average value, and SD of ratios between petrophysical parameters determined on V and H samples.

Ratio	All samples				+L samples				−L samples			
	min	max	mean	SD	min	max	mean	SD	min	max	mean	SD
Φ_V/Φ_H	0.85	1.89	1.06	0.18	0.85	1.89	1.11	0.25	0.97	1.10	1.02	0.04
K_H/K_V	0.82	15.2	3.21	3.35	0.84	15.2	4.53	4.06	0.82	7.46	1.89	1.76
$\bar{T}_{1V}/\bar{T}_{1H}$	0.68	1.50	1.01	0.19	0.71	1.50	1.05	0.20	0.68	1.25	0.97	0.18
$\bar{T}_{2V}/\bar{T}_{2H}$	0.46	2.18	1.09	0.36	0.76	2.18	1.19	0.42	0.46	1.43	0.99	0.27
ρ_V/ρ_H	0.88	2.84	1.32	0.41	0.88	2.84	1.52	0.50	0.92	1.27	1.13	0.11
m_V/m_H	0.69	1.44	1.01	0.17	0.73	1.20	0.98	0.14	0.69	1.44	1.04	0.14
$\bar{\tau}_V/\bar{\tau}_H$	0.61	3.08	1.36	0.61	0.61	2.94	1.48	0.61	0.76	3.08	1.24	0.60
$U_{\tau V}/U_{\tau H}$	0.84	1.78	1.10	0.19	0.90	1.78	1.10	0.23	0.84	1.45	1.10	0.19

$$\bar{T}_{1,2} = \exp\left(\sum_{j=1}^{n} a_j \ln(T_{1,2j}) \right) \qquad (4)$$

is determined considering the coefficients a_j as weighting factors with the sum of all weighting factors being unity.

The NMR experiments to determine the longitudinal and transversal relaxation time distribution of 53 Bahariya sandstone samples were performed in a MARAN 7 (Resonance Instruments) equipment operating at a Lamor frequency of 7 MHz. After drying at 35 °C for more than 48 hours in vacuum, the samples were saturated fully with demineralized water.

To demonstrate the influence of lamination, two pairs of samples were selected: the pair of +L samples B7H and B7V and the pair of −L samples B14H and B14V. Table 3 compiles the values of the petrophysical parameters determined for the two selected pairs of samples. The porosity values of the H and V samples of each pair are close to each other. But regarding the permeability of the +L pair, a strong anisotropy with a ratio $K_H/K_V = 9$ becomes obvious. The −L pair shows only a negligible difference in the permeability of the H and V sample. Figure 2 shows the cumulative spectra of transversal relaxation time T_2 for the four selected samples. The spectra are similar for H and V samples of both pairs. The resulting mean relaxation times $\bar{T}_1$ and $\bar{T}_2$ of the H and V samples differ only slightly within each pair (see Table 3).

Looking at Tables 1 and 2, the results of the comparison between the +L and −L pairs of samples can be generalized. A decrease of the mean relaxation times $\bar{T}_1$ and $\bar{T}_2$ is observed for the +L samples as a consequence of the reduction in porosity and permeability in comparison with the −L samples (see Table 1). The NMR relaxation time distribution is inherently a scalar property. Consequently, the mean values of the ratios $\bar{T}_{1V}/\bar{T}_{1H}$ and $\bar{T}_{2V}/\bar{T}_{2H}$, which are compiled in Table 2, are close to unity.

Figure 3 displays a comparison between the mean relaxation times $\bar{T}_1$ and $\bar{T}_2$ determined for all investigated Bahariya sandstone samples. The best fitting power-law equation with an exponent close to 1.0 confirms a linear relationship between the two quantities. The rather high $\bar{T}_1/\bar{T}_2$ ratio with an average value close to 10 is a result of the dispersed iron minerals that cause internal magnetic field gradients and stronger dephasing effects (Zhang et al., 2001). It should be noted that the MARAN 7 equipment used for our experiments operates at a 3.5 times higher magnetic field than the frequently used MARAN 2 instrument. The strong magnetic field amplifies internal gradients and causes higher $\bar{T}_1/\bar{T}_2$ ratios. Considering the strong correlation between two mean relaxation times $\bar{T}_1$ and $\bar{T}_2$, which is expressed by a coefficient of determination of $R^2 = 0.91$, it can be assumed that the two quantities reflect the variation of pore volume-to-surface ratio as indicated in equation 1 (or pore radius) in a similar way.

Spectral-induced polarization

Induced polarization (IP) is caused by electrochemical effects associated with the electrical double layer (EDL) forming on the solid-liquid interface of porous material. Various conceptual and theoretical models exist to describe this phenomenon. Some models consider the polarization of the EDL itself surrounding a mineral grain (e.g., Lesmes and Morgan, 2001), whereas others consider the polarization of pore throats because of differences in ionic mobility between wide and narrow pores (Marshall and Madden, 1959; Titov et al., 2002). An ion-sorting effect is caused also by clay minerals dispersed in the pore space of sandstones (Schön, 1996).

IP effects can be observed in the time domain by slow voltage decay after switching off the driving current signal. In the frequency domain, polarization phenomena cause a phase shift between injected current and measured voltage signal. The extension of frequency domain measurements to a wide frequency range is referred to as spectral-induced polarization (SIP). The frequency-dependent behavior of resistivity amplitude and phase shift is recorded.

The induced polarization spectra of 53 Bahariya sandstone samples were acquired in the frequency range from 2.8 mHz to 750 kHz by SIP Fuchs equipment (Radic Research, Germany). The measurements were performed under ambient conditions at a constant temperature of about 20 °C. The samples were saturated fully with a sodium-chloride solution of 0.56 grams per liter (g/l), resulting in a water conductivity of 0.1 S/m. The low salinity solution was chosen to enable a comparison of the measured spectra with those of other authors (e.g., Börner and Schön, 1991; Lesmes and Frye; 2001, Scott 2003). The electrical spectra of H and V samples have been determined in axial direction. Because a horizontal layering can be observed in the +L samples, the measurement of the V samples provides the transverse resistivity ρ_t, the resistivity perpendicular to the layering. For the measurements of the H samples, the current flow is parallel to the planes of layering. The resulting quantity is called longitudinal resistivity ρ_l. Figure 4 shows the phase angle spectra observed on the samples that have been selected for the compilation of petrophysical parameters in Table 3.

For evaluating SIP data, models are fitted to the amplitude and phase angle spectra by adjusting their parameters. Nordsiek and Weller (2008) suggested a novel approach where the measured com-

Table 3. Measured permeability K, T_1 and T_2 relaxation times, porosity ϕ and integrating Debye parameters ρ_0, m_t, $\bar{\tau}$, and U_τ for four Bahariya sandstone samples with the samples B7H and B7V being laminated samples (+L) and B14H and B14V nonlaminated (−L).

Sample	K in 10^{-15} m²	ϕ in %	$\bar{T}_1$ in ms	$\bar{T}_2$ in ms	ρ_0 in Ωm	m_t	$\bar{\tau}$ in ms	U_τ
B7H	0.244	8.00	31.9	3.04	517.62	0.269	25	1.92
B7V	0.027	8.34	32.1	2.30	760.29	0.196	72	3.42
B14H	13.52	11.39	118.8	8.19	379.97	0.061	33	2.87
B14V	14.06	11.71	120.7	10.04	390.79	0.053	26	3.14

plex resistivity spectra $\rho(\omega)$ are regarded as a superposition of Debye models

$$\rho(\omega) = \rho_0 \times \left(1 - \sum_{j=1}^{n} m_j \times \left(1 - \frac{1}{1 + i\omega\tau_j} \right) \right), \quad (5)$$

with m_j and τ_j being the parameters of a single relaxation term. Decomposition of the spectra into some Debye models results in a distribution of relaxation times which is summarized by four integrating parameters. The first parameter is the DC resistivity ρ_0 that results from the low-frequency extrapolation of the amplitude spectra. The expression ρ_0 is a common parameter that occurs in most other mathematical models describing IP spectra.
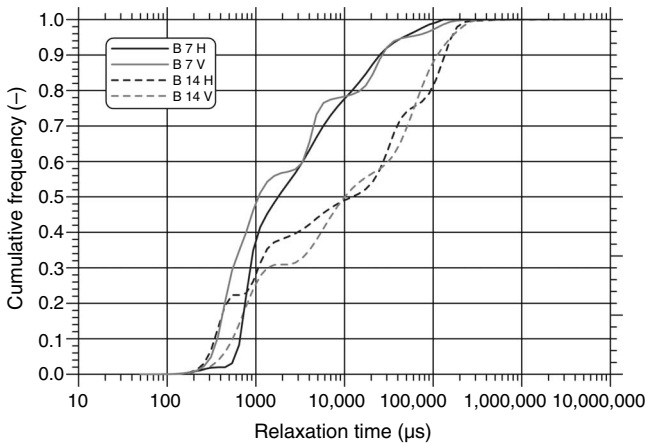
Figure 2. Cumulative curves of NMR relaxation time distributions T_2 for two pairs of Bahariya sandstone samples. B14H and B14V represent a pair of nonlaminated or isotropic samples ($-$L). B7H and B7V represent a pair of laminated samples ($+$L).
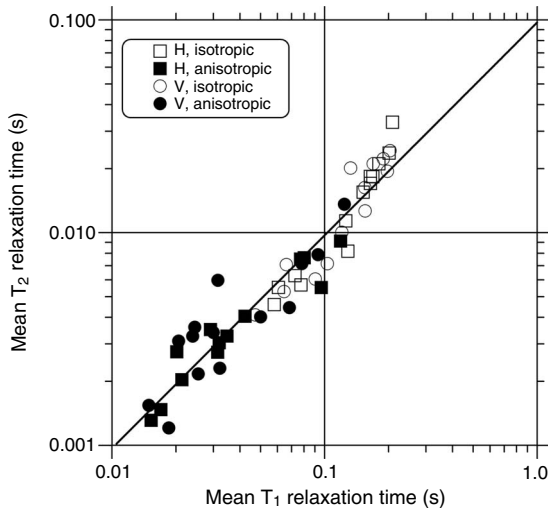

Figure 3. Comparison of mean relaxation times $\bar{T}_1$ and $\bar{T}_2$ derived from NMR measurements on Bahariya sandstones samples. The solid line represents the fitting by a power-law equation with an exponent close to 1.0 and a ratio $\bar{T}_1/\bar{T}_2$ of 10.3. The strong correlation is expressed by a coefficient of determination of $R^2 = 0.91$.

The original definition of chargeability (Sumner, 1976)

$$m = \frac{\rho_0 - \rho_\infty}{\rho_0} \quad (6)$$

quantifies the relative change of resistivity in a frequency scan with ρ_0 being the low-frequency resistivity limit and ρ_∞ the high-frequency asymptotic value. The polarization magnitude m_j computed for each individual Debye relaxation specifies the resistivity change in a narrow frequency interval. The summation across the considered frequency range yields a global polarization magnitude term, defined here as total chargeability

$$m_t = \sum_{j=1}^{n} m_j \quad (7)$$

that is considered to be the second integrating parameter of a Debye decomposition.

A relaxation time τ is used to quantify the temporal behavior of a decay process according to an exponential function $\exp(-t/\tau)$. A small relaxation time τ describes a fast decay process. The Debye decomposition assumes a temporal sequence of individual decay processes with specific relaxation times τ_j. The third integrating parameter defines the mean relaxation time

$$\bar{\tau} = \exp\left(\frac{1}{m_t} \sum_{j=1}^{n} m_j \ln(\tau_j) \right) \quad (8)$$

as the weighted logarithmic mean of all relaxation times τ_j, with the individual polarization magnitudes m_j being the weighting factors.

The fourth integrating parameter of a Debye decomposition is defined in analogy to the degree of nonuniformity of grain-size distribution curves. The nonuniformity parameter

$$U_\tau = \frac{\tau_{60}}{\tau_{10}} \quad (9)$$

characterizes the width of the relaxation time distribution, with τ_{10} and τ_{60} marking those relaxation times whereby in a cumulative curve 10% and 60% of the total chargeability is reached.
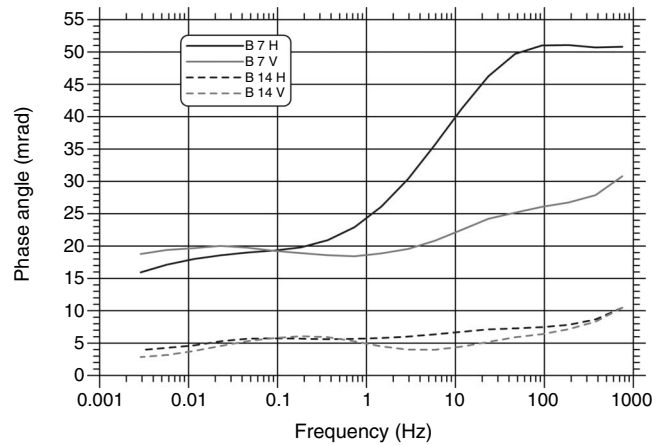

Figure 4. IP phase angle spectra of two pairs of Bahariya sandstone samples. B14H and B14V represent a pair of nonlaminated or isotropic samples ($-$L). B7H and B7V represent a pair of laminated samples ($+$L).

As an example, Figure 5 presents cumulative curves of relaxation time distribution for the two pairs of Bahariya sandstone samples that have been selected in Table 3. B14H and B14V are isotropic −L samples with similar cumulative curves. The difference in cumulative curves between H and V samples becomes obvious for the pair of anisotropic +L samples B7H and B7V. The DC resistivities determined for the H and V samples are 518 Ωm and 760 Ωm, respectively. Resistivity is known to be a directional parameter. The ratio $\rho_V/\rho_H = \rho_t/\rho_l$ quantifies the resistivity anisotropy of a pair of samples. Regarding the +L sample pair B7V and B7H, differences are observed in the other resulting integrated parameters of the Debye decomposition: total chargeability m_t, mean relaxation time $\bar{\tau}$, and the nonuniformity parameter U_τ (see Table 3). The differences in all those parameters including DC resistivity become considerably smaller for the −L pair of samples.

To decide whether the additional parameters derived from Debye decomposition vary with direction, we take a closer look at the ratios m_V/m_H, $\bar{\tau}_V/\bar{\tau}_H$, $U_{\tau \text{ V}}/U_{\tau \text{ H}}$ compiled in Table 2. The mean of the ratios m_V/m_H and $U_{\tau \text{ V}}/U_{\tau \text{ H}}$ shows values close to unity. The variation of these ratios is comparable with those of the other scalar parameters porosity Φ and mean relaxation times $\bar{T}_1$ and $\bar{T}_2$. There is no evidence from our data that m_t and U_τ reflect any directional dependence. The ratio $\bar{\tau}_V/\bar{\tau}_H$ shows a wider variation with mean values close to those of the resistivity ratio ρ_V/ρ_H. Considering that the mean value of the ratio $\bar{\tau}_V/\bar{\tau}_H$ increases for the anisotropic +L samples, a directional behavior of the mean relaxation time $\bar{\tau}$ should be assumed.

RESULTS OF PERMEABILITY ESTIMATION

Nuclear magnetic resonance

The widely applied formula for the estimation of permeability K_* from NMR relaxation measurements considers, besides the mean relaxation time, only porosity Φ:

$$K^* = a_{1,2} \times \bar{T}_{1,2_{lm}}^2 \times \Phi^4, \qquad (10)$$

with the factor $a_{1,2}$ depending on the order of magnitude of the corresponding relaxation time $T_{1,2}$. The general relation $T_1 > T_2$ leads to
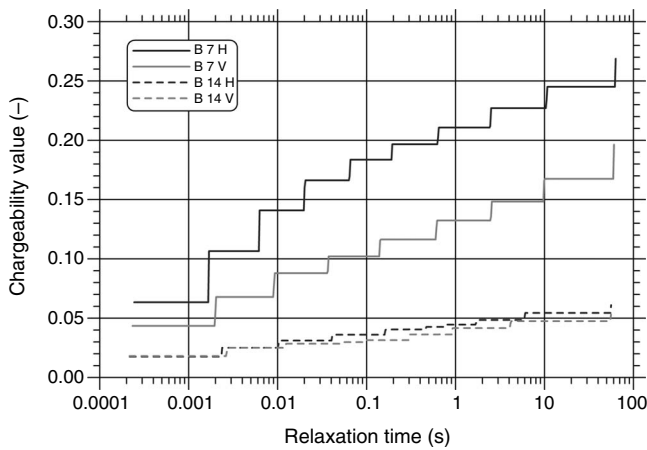
Figure 5. Cumulative curves of relaxation time distributions resulting from Debye decomposition for two pairs of Bahariya sandstone samples. The samples B14H and B14V represent the nonlaminated pair with similar cumulative curves. The difference in chargeability between horizontal (H) and vertical (V) samples becomes obvious for the laminated sample pair B7H and B7V.

$a_1 < a_2$. The exponent 2 for the relaxation time results from dimensional considerations taking into account the proportionality between pore radius and relaxation time. The porosity exponent is a result of empirical studies (Coates et al., 1999; Dunn et al., 2002).

Using our data and equation 10, the factors a_1 and a_2 have been determined by minimizing the rms

$$rms = \sqrt{\frac{1}{n}\sum_{j=1}^{n}(\log_{10}(K_j) - \log_{10}(K_j^*))^2} \qquad (11)$$

between the logarithms of measured permeability K and predicted permeability $K*$ for all $n = 53$ samples of our study. The resulting parameters are compiled in Table 4. Besides the relevant parameters resulting from regression analysis, appropriate statistical parameters, which indicate the prediction quality of the derived equations, are listed in Table 4. In addition to coefficient of determination R^2 and rms, the average deviation between calculated and measured permeability is given by

$$\bar{d} = \frac{1}{n} \times \sum_{j=1}^{n}|\log_{10}(K_j) - \log_{10}(K_j^*)|. \qquad (12)$$

The relation $a_1 < a_2$ is confirmed by our data. The independence of longitudinal relaxation from diffusion results in a slightly better permeability prediction from T_1 data, which is indicated by a higher coefficient of determination (0.788 for $\bar{T}_1$ and 0.755 for $\bar{T}_2$) and a lower average deviation (0.420 for $\bar{T}_1$ and 0.478 for $\bar{T}_2$). Figure 6 shows the comparison between the measured and predicted permeability using porosity and $\bar{T}_2$ relaxation time according to equation 10. Most of the data points of the −L samples are located close to the diagonal line that indicates a perfect permeability prediction. The two dashed lines to both sides of the diagonal indicate a deviation between measured and predicted permeability value of one order of magnitude or a factor of 10. The data points of the +L samples are scattered widely to both sides of the diagonal line, including two outliers that represent a strong underestimation of the predicted permeability.

A multivariate regression analysis with free exponents of relaxation time $\bar{T}_1$ and porosity Φ results in a slight improvement of permeability prediction by the following formula:

$$K^*_{\text{NMR}} = 1.666 \times 10^{-11}\bar{T}_1^{2.488}\Phi^{1.361} \qquad (13)$$

with $\bar{T}_1$ given in seconds (s), Φ as a fraction and K^*_{NMR} in m^2. The exponent of $\bar{T}_1$ increases from 2 to 2.5, but the porosity exponent decreases significantly from 4 to 1.36, which leads to a decrease of a_1 by two orders of magnitude. The coefficient of determination increases to 0.802, but the average deviation stays at the same level.

Considering the structure of the laminated Bahariya samples with a highly inhomogeneous susceptibility distribution at microscopic scale caused by dispersed iron minerals, an additional test of permeability prediction was made considering both relaxation times $\bar{T}_1$ and $\bar{T}_2$ with individual exponents. In this case, the exponent of $\bar{T}_1$ increases to 3.25 and the exponent of $\bar{T}_2$ becomes negative (−0.66) with the sum of the two exponents (2.59) resulting in a value close to the exponent of $\bar{T}_1$ in equation 13. The porosity exponent slightly decreases to 1.1. Regarding the strong correlation between $\bar{T}_1$ and $\bar{T}_2$ shown in Figure 3, a significant improvement of the permeability prediction could not be achieved. The coefficient of determination only slightly increases to 0.806.

In a second step, all +L samples were excluded from the data set. The parameters of all equations for permeability prediction from NMR data have been recalculated considering only the 26 nonlaminated samples which are characterized by a lower degree of anisotropy (Halisch et al., 2009). The resulting equations and the parameters quantifying the prediction quality are compiled in Table 5. A considerable decrease of the average deviation $\bar{d}$ is documented for all equations using the mean relaxation time $\bar{T}_1$. The resulting free porosity exponent c approaches the empirically determined value of 4, and the exponent b of $\bar{T}_1$ was determined with 1.56 closer to the theoretical value of 2.

Spectral-induced polarization

The parameters DC resistivity ρ_0, total chargeability m_t, and mean relaxation time $\bar{\tau}$ were derived from IP spectra of all 53 Bahariya sandstone samples. The comparison between measured permeability and the three parameters is presented in Figures 7–9. The best-fitting power-law expression shows a moderate correlation for both DC resistivity ρ_0 and total chargeability m_t with an exponent close to −5. The correlation between measured permeability and mean relaxation time $\bar{\tau}$ is rather weak. In spite of the large scatter caused by the +L samples, an inverse trend is observed.

According to the so-called PaRiS equation that has been derived from a Kozeny-Carman model considering the fractal nature of internal surface (Pape et al., 1987), the predicted permeability K^* (in mD) depends on the formation factor F and the pore surface-to-volume ratio S_{por} (in μm^{-1}):

$$K^* = 475 S_{por}^{-3.109} F^{-1}.$$ (14)

The formation factor F is defined as the ratio of the resistivity of the fully saturated sample ρ_0 and the resistivity of the saturating fluid ρ_w:

$$F = \frac{\rho_0}{\rho_w}.$$ (15)

Considering the constant fluid resistivity for all samples as regarded in this paper (10 Ωm), the formation factor is proportional to the resistivity of the saturated sample ρ_0. Therefore, the formation factor F in equation 14 can be substituted by DC resistivity ρ_0 multiplied by a constant factor.

The relationship between pore surface-to-volume ratio S_{por} and the IP effect was investigated by several authors. For soil samples, Börner et al. (1996) proposed a linear relation between S_{por} and the imaginary part of conductivity. Weller et al. (2010) confirmed this result considering an extensive database of more than 100 sandstone samples. Scott (2003) fitted generalized Cole-Cole models to spectra measured on sandstones from the UK and Germany. To characterize the IP effect, the normalized chargeability

$$m_n = \frac{m}{\rho_0}$$ (16)

is introduced describing the ratio of chargeability m to the model resistivity ρ_0. A power-law relation between pore surface-to-volume ratio S_{por} and the normalized chargeability m_n of a generalized Cole-Cole model was published by Scott (2003). The normalized chargeability m_n of the Debye decomposition approach can be determined in a similar way as the ratio of total chargeability m_t to DC resistivity ρ_0. Using an extended database, Weller et al. (2010) report a linear relationship between pore surface-to-volume ratio S_{por} and the normalized chargeability m_n derived from Debye decomposition:

$$m_n = c_s(S_{por})$$ (17)

with the factor of proportionality c_s being referred to as "polarizability of the mineral surface per unit S_{por}." Considering that single data sets do not exactly show a linear relation, a more general power law should be used to describe the relation between normalized chargeability m_n and pore surface-to-volume ratio S_{por}. Consequently, equation 14 might be modified by replacing S_{por} by a term of normalized chargeability m_n that is decomposed into $m_n = m_t \times \rho_0^{-1}$, resulting in the following proportionality

$$S_{por} \propto \left(\frac{m_t}{\rho_0}\right)^k,$$ (18)

with k being an empirical exponent. Substituting F and S_{por} in equation 14 by the terms given in equations 15 and 18, we get a general power-law equation

$$K^*_{SIP} = a \times \rho_0^b \times m_t^c$$ (19)

relating the integrating parameters ρ_0 and m_t from Debye decomposition to a predicted permeability value K^* with a, b, and c being em-

Table 4. Comparison between predicted permeability K^*_{NMR} or K^*_{SIP} and measured permeability. The factor a of all equations is determined considering $\bar{T}_1$, $\bar{T}_2$, $\bar{\tau}$ in seconds (s), Φ and m_t as a fraction, ρ_0 in Ωm and the resulting K^*_{NMR} or K^*_{SIP} in m². Data of all 53 samples are considered.

Equation	a	b	c	d	R^2	rms	$\bar{d}$
$K^*_{NMR} = a \times \bar{T}_2^2 \times \phi^4$	9.289×10^{-8}	x	x	x	0.755	0.662	0.478
$K^*_{NMR} = a \times \bar{T}_1^2 \times \phi^4$	1.578×10^{-9}	x	x	x	0.788	0.568	0.420
$K^*_{NMR} = a \times \bar{T}_1^b \times \phi^c$	1.666×10^{-11}	2.488	1.361	x	0.802	0.519	0.423
$K^*_{NMR} = a \times \bar{T}_1^b \times \phi^c \times \bar{T}_2^d$	2.438×10^{-12}	3.253	1.068	−0.664	0.806	0.514	0.420
$K^*_{SIP} = a \times \rho_0^b$	1.062×10^{-2}	−4.952	x	x	0.632	0.708	0.586
$K^*_{SIP} = a \times \rho_0^b \times m_s^c$	2.945×10^{-11}	−2.837	−3.181	x	0.815	0.502	0.418
$K^*_{SIP} = a \times \rho_0^b \times m_s^c \times \bar{\tau}^d$	3.560×10^{-12}	−2.702	−2.653	−0.858	0.846	0.458	0.384

pirical parameters which have to be adjusted by a multivariate regression analysis.

Using the Bahariya sandstone data considering all 53 samples, the relation

$$K^*_{\text{SIP}} = 2.945 \times 10^{-11} \times \rho_0^{-2.837} \times m_t^{-3.181} \qquad (20)$$

(with ρ_0 in Ωm, m_t as fraction, and K^*_{SIP} in m²) was derived resulting in a coefficient of determination $R^2 = 0.815$. In Figure 10, the permeability values K^*_{SIP} calculated from SIP data by equation 20 are plotted versus measured permeability K.

Analyzing induced polarization (IP) logs, Pape and Vogelsang (1996) found that a parameter derived from time-domain IP measurements called "extreme relaxation time" yields a strong relationship to permeability. Kemna et al. (2005) investigated sands with different grain sizes and found a correlation of hydraulic conductivity with the largest time constant resulting from fitting by a superposition of Cole-Cole models to SIP data. Pape and Vogelsang (1996),

Binley et al. (2005), Kemna et al. (2005), and Zisser et al. (2010) identified the time constant or relaxation time as a relevant parameter for permeability estimation. Besides DC resistivity ρ_0 and total chargeability m_t, the Debye decomposition of IP spectra yields a mean relaxation time $\bar{\tau}$. Considering the potential for permeability prediction of this additional parameter $\bar{\tau}$, equation 19 should be extended:

$$K^*_{\text{SIP}} = a \times \rho_0^b \times m_S^c \times \bar{\tau}^d. \qquad (21)$$

The four empirical parameters a, b, c, and d are determined by a multivariate regression analysis resulting in the equation

$$K^*_{\text{SIP}} = 3.560 \times 10^{-12} \times \rho_0^{-2.702} \times m_t^{-2.653} \times \bar{\tau}^{-0.858},$$

$$(22)$$

with the additional parameter $\bar{\tau}$ given in seconds (s). The coefficient of determination slightly increases to $R^2 = 0.846$. The negative exponents of all three parameters derived from Debye decomposition reflect the general trend shown in the graphs of Figures 7–9. The permeability values K^*_{SIP} calculated from SIP data by equation 22 are plotted versus measured permeability K in Figure 11.

INTERPRETATION AND DISCUSSION

A closer look at Table 4 reveals the limited potential of NMR for permeability prediction in the case of data sets including anisotropic samples. The classical power-law equation published by Coates et al. (1999) with the exponent 2 for the relaxation time $\bar{T}_1$ and 4 for porosity Φ causes a considerable scatter of data if measured and predicted permeabilities are compared. The coefficient of determination stays at a moderate level ($R^2 = 0.788$). The average difference between measured and predicted value $\bar{d}$ reaches 0.420 logarithmic decades or a factor of 2.63. The prediction quality becomes even worse if $\bar{T}_1$ is replaced by $\bar{T}_2$. The average deviation reaches 0.478 logarithmic decades or a factor of 3. A multivariate regression with free exponents results in a moderate increase of the coefficient of determination ($R^2 = 0.802$), but the average deviation stays at the same level. It is interesting to note that the strong effect of porosity cannot be confirmed by the results of the multivariate regression. The exponent decreases down to a value of 1.4 instead of 4. The exponent of the relaxation time $\bar{T}_1$ is slightly increased to 2.5. The joint
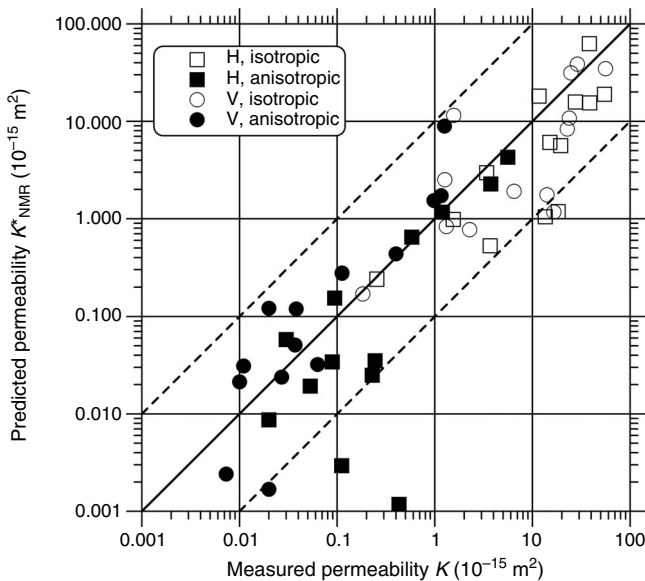

Figure 6. Permeability calculated from NMR mean relaxation time $\bar{T}_2$ and porosity Φ plotted versus permeability measured on Bahariya sandstones samples. The dashed lines indicate a distance of one decade to both sides of the measured permeability.

Table 5. Comparison between predicted permeability K^*_{NMR} or K^*_{SIP} and measured permeability K. The factor a of all equations is determined considering $\bar{T}_1$, $\bar{T}_2$, $\bar{\tau}$ in seconds (s), Φ and m_t as a fraction, ρ_0 in Ωm and the resulting K^*_{NMR} or K^*_{SIP} in m². Only data of 26 nonlaminated samples (−L) are considered.

Equation	a	b	c	d	R^2	rms	$\bar{d}$
$K^*_{\text{NMR}} = a \times \bar{T}_2^2 \times \phi^4$	9.351×10^{-8}	x	x	x	0.586	0.562	0.441
$K^*_{\text{NMR}} = a \times \bar{T}_1^2 \times \phi^4$	1.617×10^{-9}	x	x	x	0.693	0.379	0.288
$K^*_{\text{NMR}} = a \times \bar{T}_1^b \times \phi^c$	3.702×10^{-9}	1.559	4.825	x	0.705	0.368	0.286
$K^*_{\text{NMR}} = a \times \bar{T}_1^b \times \phi^c \times \bar{T}_2^d$	4.737×10^{-10}	2.906	4.644	−1.021	0.721	0.359	0.281
$K^*_{\text{SIP}} = a \times \rho_0^b$	2.862×10^{-8}	−2.586	x	x	0.358	0.544	0.415
$K^*_{\text{SIP}} = a \times \rho_0^b \times m_S^c$	3.192×10^{-12}	−2.142	−2.516	x	0.473	0.493	0.388
$K^*_{\text{SIP}} = a \times \rho_0^b \times m_S^c \times \bar{\tau}^d$	4.041×10^{-14}	−1.718	−1.516	−1.400	0.538	0.461	0.352

consideration of $\bar{T}_1$ and $\bar{T}_2$ results only in a small improvement of the predicting quality.

Considering only the more isotropic $-$L samples, the validity of the original Coates formula (equation 10) can be verified by our data. The application of a porosity exponent of 4 and a $\bar{T}_1$ exponent of 2 results in a reliable permeability prediction with a $\bar{d}$ of 0.288 which is equivalent to a factor of less than 2. The use of transversal mean re-
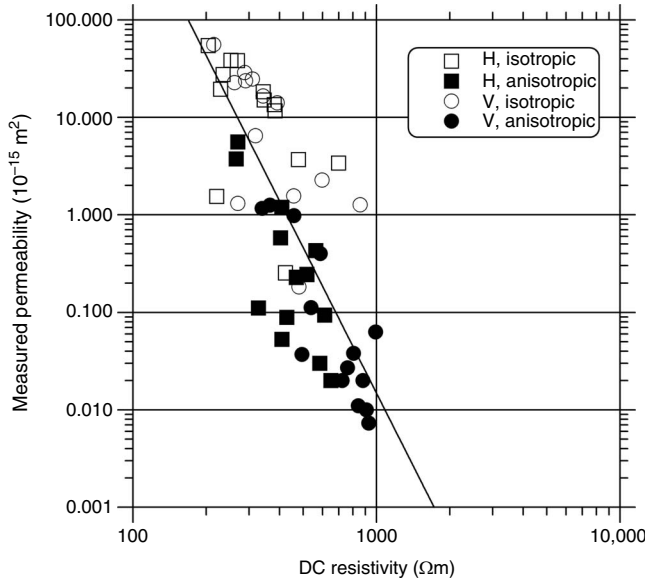
laxation time $\bar{T}_2$ instead of $\bar{T}_1$ does not result in any significant improvement of permeability prediction if only $-$L samples are considered.

An inverse relation between resistivity and permeability can be confirmed by our data (Figure 7). A similar relation with a power-law exponent of -4.41 was reported by Sawyer et al. (2001) for Appalachian reservoir rocks. Considering a constant fluid conductivity, resistivity and formation factor reflect changes in porosity according to Archie's equation (Archie, 1942). But resistivity alone cannot be

Figure 7. Comparison of measured permeability K and DC resistivity ρ_0 derived from IP spectra using Debye decomposition. All 53 Bahariya sandstone samples are included. The solid line represents the fitting by a power-law equation with an exponent of -4.95. The moderate correlation is expressed by a coefficient of determination of $R^2 = 0.63$.

Figure 9. Comparison of measured permeability K and mean relaxation time $\bar{\tau}$ derived from IP spectra using Debye decomposition. All 53 Bahariya sandstone samples are included. The solid line represents the fitting by a power-law equation with an exponent of -2.50. The weak correlation is expressed by a coefficient of determination of $R^2 = 0.36$.
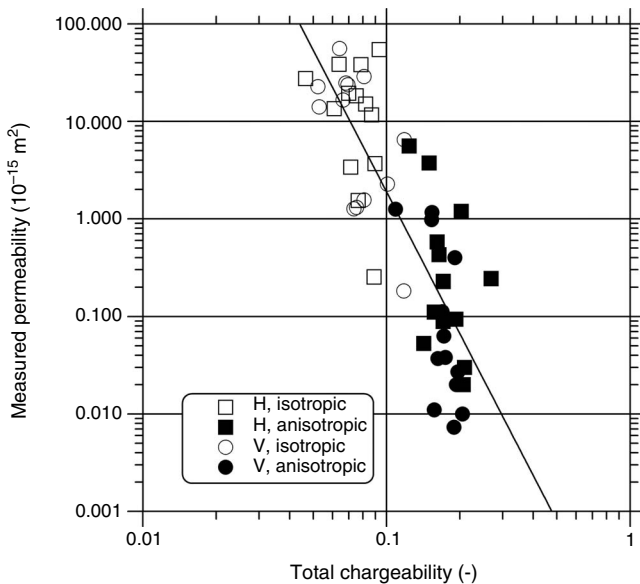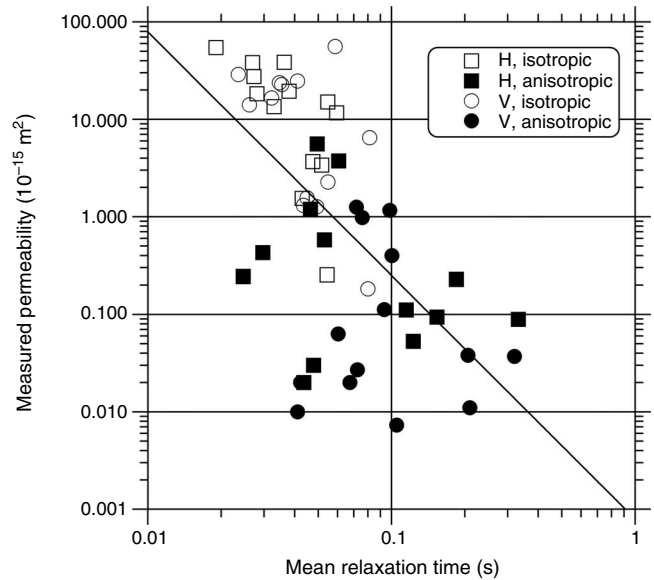

Figure 8. Comparison of measured permeability K and total chargeability m_t derived from IP spectra using Debye decomposition. All 53 Bahariya sandstone samples are included. The solid line represents the fitting by a power-law equation with an exponent of -4.83. The moderate correlation is expressed by a coefficient of determination of $R^2 = 0.69$.
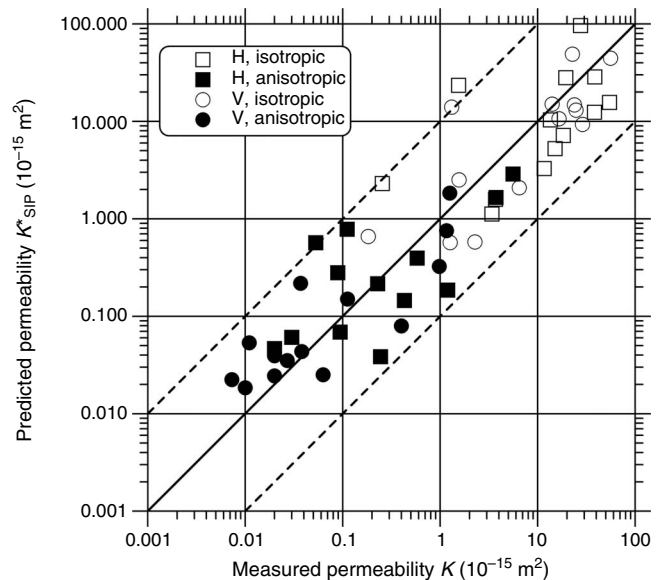

Figure 10. Permeability calculated from integrating parameters ρ_0 and m_t resulting from Debye decomposition of SIP data plotted versus measured permeability for 53 Bahariya sandstone samples.

Weller et al.

used to get a reliable permeability prediction. As in Kozeny-Carman models, an additional parameter is needed to provide information on the average pore size.

Regarding the results of earlier studies, it might be assumed that total chargeability m_t and mean relaxation time $\bar{\tau}$ are linked to pore size or specific internal surface. Using the three integrating parameters ρ_0, m_t, and $\bar{\tau}$, a quantitatively improved permeability prediction can be achieved. The coefficient of determination reaches a value of 0.846 and the average deviation $\bar{d}$ decreases at 0.384 decades. Looking at Figure 11, it becomes obvious that with the exception of one sample, all predicted permeability values are in a range with a maximum deviation of one order of magnitude. For most samples, a close agreement between measured and predicted values is achieved.

The exclusion of all +L samples results in modified formulas which are compiled in Table 5. Regarding the average deviation $\bar{d}$, only a slight improvement can be observed. Because not only the number of samples, but the interval of permeability variation decreases, the coefficients of determination decrease as well. In contrast to NMR, the general predictive power of SIP data will not increase if only −L samples are considered.

Beside electrical resistivity ρ_0, mean relaxation time $\bar{\tau}$ is identified as another directional parameter that can be determined from spectral IP data. The inverse trend reflecting a permeability decrease with a relaxation time increase, which becomes visible in Figure 9, contradicts findings of Scott (2003), Binley et al. (2005), and Zisser et al. (2010). They report an increase of time constant (or median relaxation time) with modal pore throat size or an effective hydraulic length of their samples. The wider pore space results in a permeability increase. The directional behavior of mean relaxation time as observed for our samples cannot be explained by its relation to modal pore throat size.
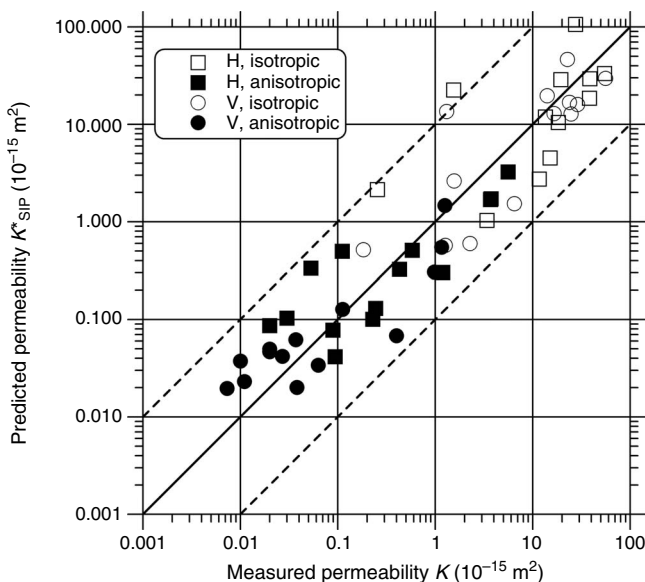

Figure 11. Permeability calculated from integrating parameters ρ_0, m_t, and $\bar{\tau}$ resulting from Debye decomposition of SIP data plotted versus measured permeability for 53 Bahariya sandstone samples.

In a recent paper considering an extended database, Kruschwitz et al. (2010) found that the positive correlation between modal pore throat and time constant is valid only for samples of relative large pores ($>10~\mu$m). For media with pore structures dominated by small pore throats, they observed relatively long time constants that are not controlled by modal pore throat size. Following the explanations given by Titov et al. (2010), the increase in relaxation time is related to "slow" diffusion processes caused by surface tortuosity and geometry of clay-filled pores. They identified low diffusivity values for their clayey sandstones.

Though the modal pore throat size has not been determined for our clayey Bahariya samples, it can be concluded from the $K - \bar{\tau}$ relation in Figure 9 that they are characterized by small pore throats and low diffusivity. The anisotropy of resistivity and permeability is caused by increased tortuosity of the V samples in comparison with the H samples. It can be assumed that the increased tortuosity in the vertical direction results in an elongation of the diffusion paths that cause rising mean relaxation times. This assumption is in agreement with a ratio $\bar{\tau}_V/\bar{\tau}_H > 1$ that has been observed for most of our sample pairs (Table 2). Our data show that because of its directional dependence and its relation to tortuosity, the mean relaxation time $\bar{\tau}$ might be well integrated in equations for assessing permeability of clayey sandstones.

The relaxation times determined by NMR do not depend on the orientation of the sample. In contrast to the directional parameters that can be used to quantify anisotropy, the relaxation times $\bar{T}_1$ and $\bar{T}_2$ are scalar parameters like density and porosity. The compilation in Table 3 shows that even for the anisotropic sample pair B7H and B7V, the experimentally determined relaxation times for the H and V samples are close to each other, whereas parameters determined from SIP and gas permeability experiments differ significantly. From the theoretical viewpoint, a correct prediction of a directional parameter like permeability from scalar quantities is possible only for isotropic material. The moderate quality of permeability estimation from NMR is caused by the anisotropy of a considerable part of samples. The parameters porosity and relaxation time do not reflect the anisotropy of the sample. Consequently, all equations based only on these parameters will fail to predict directional parameters of anisotropic material. This seems to be the main reason for a restricted applicability of NMR for permeability prediction of anisotropic samples. Only excluding the +L samples, the predicting power of the Coates formula can be confirmed for isotropic samples.

The relations based on SIP provide a better potential for a reliable permeability estimation of anisotropic samples because the parameters resistivity ρ_0 and mean relaxation time $\bar{\tau}$ consider the anisotropy of the sample. The superiority of SIP is confirmed by our data. The remaining discrepancies between predicted and measured permeability are caused by inaccuracies in the determination of permeability and IP parameters, as well as differences in the effect of pore space geometry on electrical current and gas flow. The applicability of the resulting special equations is restricted to sandstone samples of the Bahariya Formation. Like other empirical petrophysical equations, the free factors and exponents have to be adjusted for different lithological units.

Because NMR logging tools provide only a permeability of isotropic formations, the directional dependence can only be explored by other methods. Schön et al. (2003) present an algorithm that includes multicomponent induction resistivity data to predict the directional dependence of permeability. A combination of NMR and

resistivity techniques including SIP provides the potential for further improvement in permeability prediction.

CONCLUSIONS

The set of sandstone samples of the Bahariya Formation with a variation of permeability over four orders of magnitude has proven to be appropriate to compare the applicability of known and generalized relations for permeability prediction from NMR and SIP data.

NMR is a widely acknowledged method for permeability prediction. Our investigation has shown that the known power-law relations based on porosity and relaxation time provide only a moderate accuracy if anisotropic samples are included. A multivariate regression that enables a free choice of the exponents does not result in a significant improvement of the prediction quality. The anisotropy of the samples has been identified as the main reason for the restricted applicability. Both initial parameters in the power-law relation, porosity and mean relaxation time, are scalar quantities that do not consider the anisotropy of the samples.

Several authors have demonstrated the potential of SIP for permeability prediction. There is a wide variation of parameters derived from IP spectra. The parameters strongly depend on the fitting model (e.g., Cole-Cole type models or constant phase angle model). Because the model should be chosen in accordance with the special shape of the spectra, the resulting relations are restricted in their applicability.

The Debye decomposition is a general approach that enables a good fitting for all types of spectra. The resulting sequence of relaxation times and chargeabilities yields the integrating parameters DC resistivity, total chargeability, and mean relaxation time. These parameters, which are derived from directional SIP measurements, are used in a general power-law equation for permeability estimation. The comparison of measured and predicted permeability values proves the applicability for isotropic and anisotropic samples.

More suitable data sets from samples of different lithologies including carbonates are required to validate and generalize the presented approach of permeability prediction from IP spectra.

ACKNOWLEDGMENTS

REFERENCES

Archie, G. E., 1942, The electrical resistivity log as an aid in determining some reservoir characteristics: Transactions of the American Institute of Mining, Metallurgical and Petroleum Engineers, **146**, 54–62.

Binley, A., L. D. Slater, M. Fukes, and G. Cassiani, 2005, Relationship between spectral induced polarization and hydraulic properties of saturated and unsaturated sandstone: Water Resources Research, **41**, W12417, doi: 10.1029/2005WR004202.

Börner, F. D., and J. H. Schön, 1991, A relation between the quadrature component of electrical conductivity and the specific surface area of sedimentary rocks: The Log Analyst, **32**, 612–613.

Börner, F. D., J. R. Schopper, and A. Weller, 1996, Evaluation of transport and storage properties in the soil and groundwater zone from induced polarization measurements: Geophysical Prospecting, **44**, 583–601, doi: 10.1111/j.1365-2478.1996.tb00167.x.

Carr, H. Y., and E. M. Purcell, 1954, Effects of diffusion on free precession in nuclear magnetic resonance experiments: Physical Review, **94**, 630–638, doi: 10.1103/PhysRev.94.630.

Coates, G. R., H. J. Vinegar, P. N. Tutunjian, and J. S. Gardner, 1993, Restrictive diffusion from uniform gradient NMR well logging: 68th Annual Technical Conference and Exhibition of the Society of Petroleum Engineers, paper SPE 26472.

Coates, G. R., L. Xiao, and M. G. Prammer, 1999, NMR logging principles and applications: Halliburton Energy Services, Houston.

Dunn, K.-J., D. J. Bergman, G. A. Latorraca, 2002, Nuclear magnetic resonance: Petrophysical and logging applications, *in* K. Helbig and S. Treitel, eds., Handbook of geophysical exploration, Seismic exploration series, Vol. 32, Pergamon.

Halisch, M., A. Weller, C.-D. Sattler, W. Debschütz, and A. M. El-Sayed, 2009, A complex core-log case study of an anisotropic sandstone, originating from Bahariya Formation, Abu Gharadig Basin, Egypt: Petrophysics, **50**, 478–497.

Hördt, A., A. Druiventak, R. Blaschek, F. Binot, A. Kemna, P. Kreye, and N. Zisser, 2009, Case histories of hydraulic conductivity estimation with induced polarization at the field scale: Near Surface Geophysics, **7**, 529–545.

Kemna, A., H.-M. Münch, K. Titov, E. Zimmermann, and H. Vereecken, 2005, Relation of SIP relaxation time of sands to salinity, grain size and hydraulic conductivity: 11th European Meeting of Environmental and Engineering Geophysics of the Near Surface Geoscience Division, EAGE, Abstract P054.

Kruschwitz, S., A. Binley, D. Lesmes, and A. Elshenawy, 2010, Textural controls on low frequency electrical spectra of porous media: Geophysics, **75**, no. 4, WA113–WA123, doi: 10.1190/1.3479835.

Lesmes, D. P., and K. M. Frye, 2001, Influence of pore fluid chemistry on the complex conductivity and induced-polarization responses of Berea sandstone: Journal of Geophysical Research, **106**, 4079–4090, doi: 10.1029/2000JB900392.

Lesmes, D. P., and F. D. Morgan, 2001, Dielectric spectroscopy of sedimentary rocks: Journal of Geophysical Research, **106**, 13329–13346, doi: 10.1029/2000JB900402.

Marshall, D. J., and T. R. Madden, 1959, Induced polarization, a study of its causes: Geophysics, **24**, 790–816, doi: 10.1190/1.1438659.

Meiboom, S., and D. Gill, 1958, Modified spin-echo method for measuring nuclear relaxation times: Review of Scientific Instruments, **29**, 688–691, doi: 10.1063/1.1716296.

Nordsiek, S., and A. Weller, 2008, A new approach to fitting induced-polarization spectra: Geophysics, **73**, no. 6, F235–F245, doi: 10.1190/1.2987412.

Pape, H., L. Riepe, and J. R. Schopper, 1987, Theory of self-similar network structures in sedimentary and igneous rocks and their investigation with microscopical and physical methods. Journal of Microscopy, **148**, 121–147.

Pape, H., and D. Vogelsang, 1996, Fractal evaluation of induced polarization logs in the KTB-Oberpfalz HB, Bundesanstalt für Geowissenschaften und Rohstoffe/Geologische Landesämter in der Bundesrepublik Deutschland: Geologisches Jahrbuch, **54** (E), 3–27.

Sawyer, W. K., C. I. Pierce, and R. B. Lowe, 2001, Electrical and hydraulic flow properties of Appalachian petroleum reservoir rocks: Petrophysics, **42**, 71–82.

Scheidegger, A. E., 1957, Physics of flow through porous media: University of Toronto Press.

Schön, J. H., 1996, Physical properties of rocks: Fundamentals and principles of petrophysics, Handbook of geophysical exploration, Seismic exploration series, Vol. 18, Pergamon.

Schön, J. H., D. T. Georgi, and O. Fanini, 2003, Imparting directional dependence on log-derived permeability: Society of Petroleum Engineers, paper 82058, 48–56, doi: 10.2118/82058-PA.

Scott, J. B. T., 2003, Low-frequency electrical spectroscopy of sandstone: Ph.D. thesis, University of Birmingham, Birmingham, UK.

Slater, L. D., and D. R. Glaser, 2003, Controls on induced polarization in sandy unconsolidated sediments and application to aquifer characterization: Geophysics, **68**, 1547–1558, doi: 10.1190/1.1620628.

Straley, C., D. Rossini, A. Vinegar, P. N. Tutunjian, and C. E. Morriss, 1997, Core analysis by low-field NMR: The Log Analyst, **38**, 84–94.

Sumner, J. S., 1976, Principles of induced polarization for geophysical exploration: Elsevier, Amsterdam.

Titov, K., V. Komarov, V. Tarasov, and A. Levitski, 2002, Theoretical and experimental study of time domain-induced polarization in water-saturated

sands: Journal of Applied Geophysics, **50**, 417–433, doi: 10.1016/S0926-9851(02)00168-4.

Titov, K., A. Tarasov, Y. Ilyin, N. Seleznev, and A. Boyd, 2010, Relationships between induced polarization relaxation time and hydraulic properties of sandstone: Geophysical Journal International, **180**, 1095–1106, doi: 10.1111/j.1365-246X.2009.04465.x.

Weller, A., and F. D. Börner, 1996, Measurements of spectral induced polarization for environmental purposes: Environmental Geology, **27**, 329–334, doi: 10.1007/BF00766702.

Weller, A., L. Slater, S. Nordsiek, and D. Ntarlagiannis, 2010, On the estimation of specific surface per unit pore volume from induced polarization: A robust empirical relation fits multiple data sets: Geophysics, **75**, no. 4, WA105–WA112, doi: 10.1190/1.3471577.

Zhang, G. Q., G. J. Hirasaki, and W. V. House, 2001, Effect of internal field gradients on NMR measurements: Petrophysics, **42**, 37–47.

Zisser, N., A. Kemna, and G. Nover, 2010, Relationship between low-frequency electrical properties and hydraulic permeability of low-permeability sandstones: Geophysics, **75**, no. 3, E131–E141, doi: 10.1190/1.3413260.

Zisser, N., and G. Nover, 2009, Anisotropy of permeability and complex resistivity of tight sandstones subjected to hydrostatic pressure: Journal of Applied Geophysics, **68**, no. 3, 356–370, doi: 10.1016/j.jappgeo.2009.02.010.